THE JOURNAL OF BIOLOGICAL CHEMISTRY VOL. 283, NO. 49, pp. 34121–34128, December 5, 2008

Experimental Investigation of the Seesaw Mechanism of the Relay Region That Moves the Myosin Lever Arm*[S]

Received for publication, July 30, 2008, and in revised form, September 29, 2008 Published, JBC Papers in Press, October 14, 2008, DOI 10.1074/jbc.M805848200

Bálint Kintses, Zhenhui Yang, and András Málnási-Csizmadia[1]

From the Department of Biochemistry, Eötvös Loránd University, Budapest H-1117, Hungary

A seesaw-like movement of the relay region upon the recovery step of myosin was recently simulated *in silico*. In this model the relay helix tilts around its pivoting point formed by a phenylalanine cluster (Phe^{481}, Phe^{482}, and Phe^{652}), which moves the lever arm of myosin. To study the effect of the elimination of the proposed pivoting point, these phenylalanines were mutated to alanines in two *Dictyostelium* myosin II motor domain constructs ($M_{F481A,\ F482A}$ and M_{F652A}). The relay movement was followed by the fluorescence change of Trp^{501} located in the relay region. The steady-state and transient kinetic fluorescence experiments showed that the lack of the phenylalanine fulcrum perturbs the formation of the "up" lever arm state, and only moderate effects were found in the nucleotide binding, the formation of the "down" lever arm position, and the ATP hydrolysis steps. We conclude that the lack of the fulcrum decouples the distal part of the relay from the nucleotide binding site upon the recovery step. Our molecular dynamics simulations also showed that the conformation of the motor is not perturbed by the mutation in the down lever arm state, however, the lack of the pivoting point rearranges the dynamic pattern of the kink region of the relay helix.

Myosins are ATP-driven molecular motors that generate force and move along actin filaments. When ATP binds to the actomyosin complex, the first switch 1 loop closes, which opens the actin-binding cleft, causing actomyosin dissociation (1–4). It is followed by a rapid equilibrium step called the recovery step (5, 6), when the closure of the switch 2 loop drives a 65° rotation of the converter/lever arm region placing the lever arm to the "up" position (7, 8). Recently, several computer simulations have been published on the analysis of the recovery step (9–13). Fischer *et al.* (9) composed a model that describes the structural transition between the pre- and post-recovery states (down and up lever arm states, respectively) by simulating the intermediate structures using an unconstrained minimum-energy pathway method. The resulting structural trajectory shows that the relay helix moves in a seesaw-like fashion coupling the movement of switch 2 and the rotation of the lever arm: the closure of switch 2 pulls down the relay helix near its N-terminal end and due to a fulcrum in the middle of the helix, serving as the pivoting point, the C-terminal end of the relay helix swings upwards and finally unwinds in a second phase (Fig. 1). Molecular dynamics simulations confirmed the seesaw-like motion and the pivoting role of this hydrophobic fulcrum (11, 12), however, experimental validation is still lacking.

The recovery step is an experimentally well characterized process by the fluorescence change of the conserved Trp^{501} (*Dictyostelium* numbering, homologous to Trp^{510} in rabbit skeletal myosin), which is located at the C-terminal end of the relay helix (5). Scheme 1 shows the reaction steps of the myosin basal ATPase cycle characterized by the use of a mutant motor domain, containing a single Trp^{501} (M_{W501+} construct) (14). Steps 1 and 2 (K_1K_2 in Scheme 1) represent a two-step induced-fit ATP binding process. M†·ATP, which has a 20% lower fluorescence than the M apo state (Protein Data Bank code 1q5g), corresponds to the down lever arm state (*i.e.* pre-recovery, open, post-rigor; PDB 1FMW and 1MMD). This state has an open switch 2 and thus the lever arm is in the down orientation. The ATP binding process is followed by the recovery step (step 3a in Scheme 1) when switch 2 loop closes and the relay/converter/lever arm region rotates into the up lever arm state (*i.e.* post-recovery, pre-power stroke state; M*·ATP in Scheme 1, PDB codes 1VOM and 1MND (7). Note that in the post-recovery state myosin contains ATP, whereas in the pre-power stroke state it has ADP·P_i, however, there structures are similar.). The closed switch 2 is required for the hydrolysis of ATP (15, 16). The forward direction of the recovery step results in a 110% fluorescence emission intensity increase of Trp^{501}, serving a useful signal to follow the conformational change in the relay/converter region.

This article demonstrates experimental investigations on the role of the relay helix fulcrum during the recovery step. This hydrophobic fulcrum is formed mainly by three conserved phenylalanine residues: Phe^{652} (part of the central β-sheet), Phe^{481} and Phe^{482} (relay helix). Two mutant constructs were produced in the M_{W501+} construct, in which different parts of the fulcrum were replaced with alanines. $M_{F481A,\ F482A}$ construct has a reduced fulcrum in the side of the relay helix, whereas M_{F652A} contains a reduced support for the relay helix. The steady-state and transient kinetic measurements show that the three phenylalanines form a real functional unit because the functional properties of the two constructs were very similar to each other. The mutations cause very specific changes in the mechanism of the basal ATPase cycle. No change was detected in the conformations of the apo and the down lever arm states, but a dramatic effect was found in the formation of the up lever arm state

* This work was supported by The European Research Council under the European Community's Seventh Framework Program FP7/2007–2013/ERC Grant 208319. The costs of publication of this article were defrayed in part by the payment of page charges. This article must therefore be hereby marked "*advertisement*" in accordance with 18 U.S.C. Section 1734 solely to indicate this fact.

[S] The on-line version of this article (available at http://www.jbc.org) contains supplemental Figs. S1–S11.

[1] To whom correspondence should be addressed. Tel.: 36-1-209-0555 (ext. 8780); Fax: 36-1-381-2172; E-mail: malna@.elte.hu.

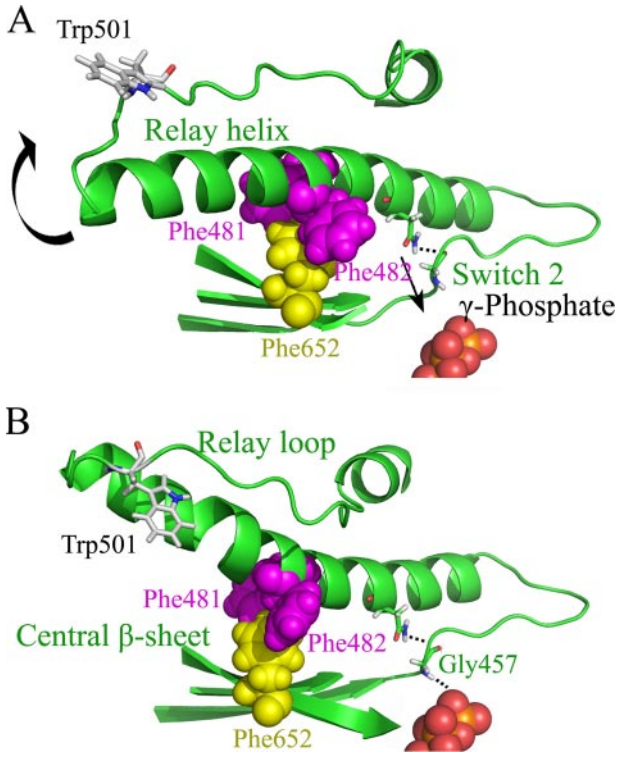

FIGURE 1. **The relay-helix seesaw mechanism during the recovery step, which couples the closing of switch 2 and the rotation of the converter-domain/lever arm region.** *A*, the down lever arm conformation; and *B*, the up lever arm step conformation after molecular dynamics simulation. In the recovery step, first Gly^{457} (switch 2) moves toward the γ-phosphate of ATP, thus pulling down the relay helix via a hydrogen bond. As a result the other (C-terminal) end of the relay helix moves upwards and in a second phase unwinds. The pivoting point of the seesaw is highlighted by spacefill modeling (Phe^{652} in *yellow* and Phe^{481} and Phe^{482} in *purple*). Trp^{501} is highlighted by stick representation. Because the relay loop and thus Trp^{501} is missing in the original pre-recovery structure, it is modeled.

$$M + ATP \underset{}{\overset{K_1K_2}{\rightleftharpoons}} M^{\dagger}.ATP \underset{}{\overset{K_{3a}}{\rightleftharpoons}} M^{*}.ATP \underset{}{\overset{K_{3b}}{\rightleftharpoons}} M^{*}.ADP.P_i$$

ATP binding; recovery step; hydrolysis

$$M^{\dagger}.ADP.P_i \underset{}{\overset{\text{reverse recovery step } K_4}{\rightleftharpoons}} M^{\dagger}.ADP + P_i$$

$$M + ADP \underset{K_6K_7}{\overset{\text{product release steps}}{\rightleftharpoons}} M^{\dagger}.ADP + P_i \underset{K_5}{\overset{}{\rightleftharpoons}} M^{\dagger}.ADP.P_i$$

SCHEME 1

(step 3a). K_{3a} is dramatically reduced and the conformation of this state is perturbed. In good agreement with these experimental results our molecular dynamics simulations show that the mutations changed the conformation of the relay region only in the up lever arm state. Interestingly, we also found that the mutations cause site-specific dynamic changes of the relay helix unwinding region in the down lever arm state without significant conformational change. This effect could be an indication of the reaction trajectory perturbation in the recovery step.

EXPERIMENTAL PROCEDURES

All chemical reagents were purchased from Sigma, except nucleotides (Roche Applied Sciences) and 3′-(*N*-methyl-anthraniloyl)-2′-deoxy-ATP (Jena Bioscience GmbH, Germany) and [γ-^{32}P]ATP (Izinta Ltd., Hungary).

Protein Engineering, Expression, and Purification—F481A/F482A or F652A mutations were introduced into the single tryptophan containing W501+ *Dd* myosin motor domain II M761 cDNA fragment (14). Recombinant proteins were expressed in Dd AX2-ORF+ cells and purified using His-tagged chromatography as described previously (14). Preparations were dialyzed against an assay buffer (40 mM NaCl, 20 mM HEPES, pH 7.3, 2 mM MgCl, and 2 mM mercaptoethanol), in which all experiments were performed. Actin preparation and pyrene labeling were done as described previously (17).

Steady-state Fluorescence Measurements—These measurements were carried out with a Fluoromax Spex-320 fluorimeter equipped with a 150-watt Xe lamp. Tryptophan was excited at 296 nm with 2-nm bandwidth excitation and emission slits and fluorescence was detected in 310–420 nm range at 20 and 6 °C. During acrylamide quenching experiments the time courses of tryptophan fluorescence were detected at 340 nm and the 3 μM motor domains were titrated with acrylamide in a 0.05–0.4 mM concentration range.

Stopped-flow Measurements—The stopped-flow measurements were carried out on a KinTek SF-2004 (KinTec Corporation) or on a BioLogic SFM-300/400 (BioLogic SAS, France) stopped-flow fluorimeter, both equipped with 150-watt Superquiet Hg-Xe lamps (Hamamatsu Photonics, UK). Tryptophan was excited at 297 nm, slits were 4 nm and a 340-nm interference filter (Corion CFS-001999 9L134) was used on the emission side. Pyrene was excited at 365 nm and fluorescence was detected with a WG420 cut-off filter (Comar Instruments, UK). The dead time of the KinTec SF-2004 was determined to be 1 ms at 18 ml/s flow rate, the BioLogic stopped-flow has 0.2- and 2-ms dead time with the μFC-08 cuvette and FC-15 cuvette, respectively, at the same flow rate. All concentrations noted are post-mix concentrations, and all experiments were carried out at 20 °C, unless otherwise stated.

Quench-flow Experiments—The quench-flow experiments were carried out on a RQF-3 quench-flow apparatus (KinTec Corporation) using [γ-^{32}P]ATP radioactive nucleotide. Samples were handled as in Ref. 18 and the radioactivity of the γ-^{32}P-hydrolytic product was measured with a Wallac 1409 Liquid Scintillation Counter (PerkinElmer Life Sciences). The indicated concentrations are post-mix concentrations.

Actin-activated ATPase—The actin-activated ATPase were determined by the use of a pyruvate kinase/lactate dehydrogenase-coupled assay as described earlier (19) in buffer containing 5 mM HEPES, pH 7.2, 1 mM MgCl, 1 mM KCl.

Molecular Dynamics Simulation—For the molecular dynamics simulations two *Dictyostelium* myosin II motor domain crystal structures were prepared. InsightII 2000 software was used for generating the missing parts of 1MMD (pre-recovery (up lever arm) structure). The ADP·BeF_x located in the nucleotide binding site was replaced with ATP by changing the BeF_x to phosphate group. Then equilibrium molecular dynamics simulation was performed to achieve relaxed conformations and by averaging the coordinates of 125 structures picked up at each 2-ps time point of the equilibrium phase, we visualized a relaxed conformation. For the up lever arm state we used a

structure from Jon Kull,[2] which has exactly the same conformation as 1VOM, and just contains all of the residues. In this structure the BeF_x was also replaced by the phosphate group. Mutations F481A, F482A, or F652A were introduced into these structures and further molecular dynamics simulation were done in the same way. Constant volume periodic boundaries were used with the box dimensions of 134.7 Å. Then the structures were solvated by TIP3P water with a 12-Å cut-off value. Finally, the system was mechanically minimized with parm03 parameters and equilibrated for 2 ns at 300 K by the SHAKE algorithm with 2-fs time steps in the AMBER9 program. Temperature control parameters were set up based on the method of Berendsen (26). We determined the amplitude (δ) of the torsional mobility of the Φ, Ψ angles according to Equation 1,

$$\delta = \sqrt{\frac{\Sigma(x - \bar{x})^2}{n - 1}} \qquad \text{(Eq. 1)}$$

where x is the actual torsion angle, [overbar]x *is* the average of all the Φ or Ψ angles of the given residue, and n the number of data points. The experiments were repeated three times and averaged, each based on 125 collected structures picked up at each 2-ps time point from 250-ps long equilibrium phases.

RESULTS

Steady-state Fluorescence of $M_{F481A,\ F482A}$ and M_{F652A}—The effects of the mutations on the steady-state fluorescence emission spectra of Trp^{501} were studied by comparing $M_{F481A,\ F482A}$ and M_{F652A} to the M_{W501+} in the presence of different nucleotides at 20 °C (Fig. 2). In the absence of nucleotide the three constructs have similar emission spectra (emission maximum at 342 nm). Also, the fluorescence spectra of the mutants were identical to that of M_{W501+} in the presence of ADP (15% quenches and 2-nm blue shifts compared with the apo states). On addition of ATP the mutants show decreased fluorescence enhancements compared with the M_{W501+}. Although the fluorescence of M_{W501+} increases by 100% compared with the ADP-bound fluorescence level (14), the fluorescence intensity increases of $M_{F481A,\ F482A}$ and M_{F652A} were only 10 and 5%, respectively. These observations have raised the question, whether the smaller fluorescence enhancements of the mutants are due to the formation of new fluorescent states, or just K_{3a} of the mutants are pulled to the $M^{\dagger}ATP$ states. The comparison of the fluorescence intensities of the ADP·AlF_4-bound forms answers this question, because the ADP·AlF_4 induces the up lever arm state of myosin, which is the high fluorescence state of M_{W501+}. Fig. 2 shows that, whereas the fluorescence level of the M_{W501+}·ADP·AlF_4 state is 110% higher than the M_{W501+}·ADP state, that of the $M_{F481A,F482A}$·ADP·AlF_4 and M_{F652A}·ADP·AlF_4 are just 40 and 35% higher, respectively. To demonstrate that the ADP·AlF_4-bound mutant constructs are also single fluorescent states just as M_{W501+}·ADP·AlF_4 (5) and not a mixture of the low and high fluorescent states of M_{W501+}, the temperature dependence of the fluorescence emissions were determined (see supplemental Fig. S1). Because the relative fluorescence intensities of the apo, ADP-, and ADP·AlF_4-bound forms were not influenced by temperature and the former states are known to be single fluorescent states, $M_{F481A,F482A}$·ADP·AlF_4 and M_{F652A}·ADP·AlF_4 populate predominantly a single fluorescent state, which is structurally different from the wild type up lever arm state (M_{W501+}·ADP·AlF_4).

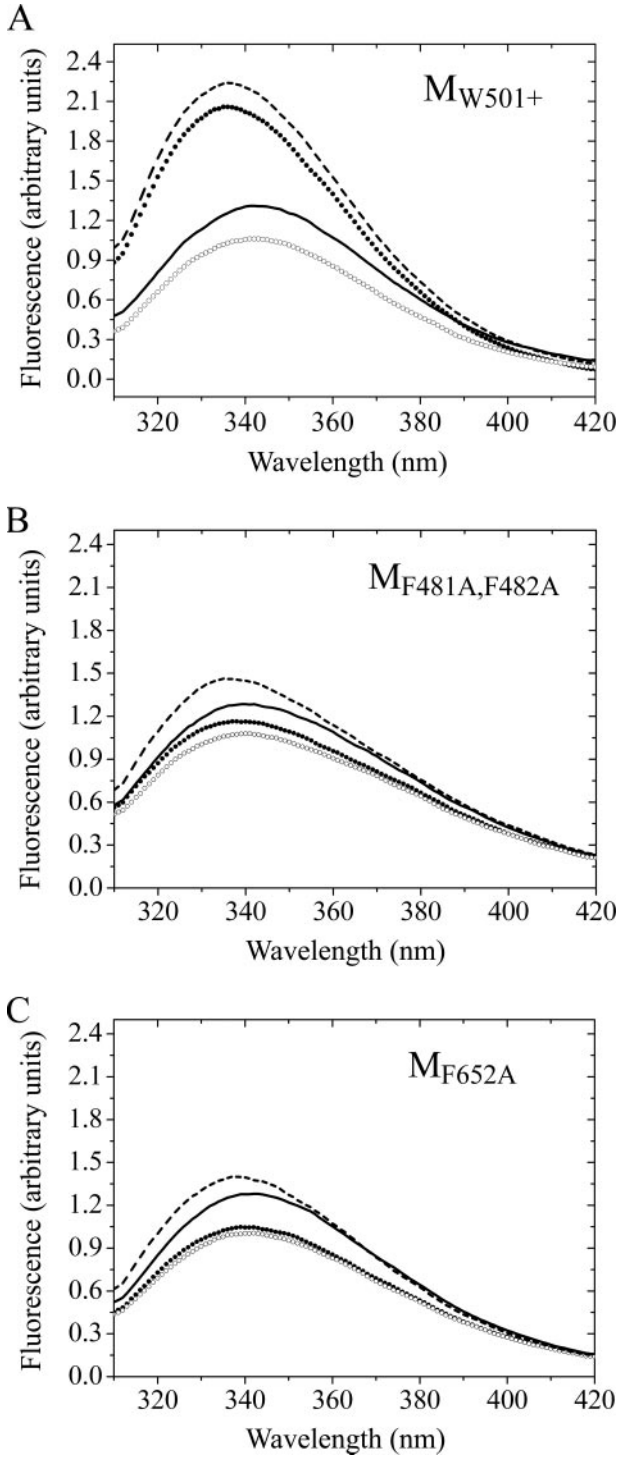

FIGURE 2. **Fluorescence emission spectra of 3 μM M_{W501+} (*A*), $M_{F481A,\ F482A}$ (*B*), and M_{F652A} (*C*) in the absence (—) and presence of 0.5 mM ADP (○), 0.5 mM ATP (●), or ADP·AlF_4 (- - -) at 20 °C.** ADP·AlF_4 complex was made by addition of 100 μM $AlCl_3$ and 4 mM NaF to myosin-ADP and incubated overnight before measurement. Tryptophan was excited at 297 nm.

Acrylamide Quenching Experiment—To explore the possible structural differences between the ADP·AlF_4-bound forms of

[2] J. Kull, unpublished data.

TABLE 1

Stern-Volmer constants of the acrylamide quenching experiments

3 μM M_{W501+}, $M_{F481A,\ F482A}$, and M_{F652A} were titrated with up to 0.4 M acrylamide in the absence and presence of different nucleotides at 20 °C (supplemental Fig. S2). In M_{W501+} the difference in the Stern-Volmer constants of the "up" (ADP·AlF_4) and the "down" (ADP) lever arm states is significantly larger than the mutants'.

Nucleotide	Stern-Volmer constant (M^{-1})		
	M_{W501+}	$M_{F481A,\ F482A}$	M_{F652A}
None	4.11 ± 0.09	4.10 ± 0.08	3.77 ± 0.08
ADP	3.73 ± 0.07	3.70 ± 0.08	3.34 ± 0.12
ATP	3.20 ± 0.08	3.74 ± 0.08	3.26 ± 0.10
ADP·AlF_4	2.98 ± 0.04	3.58 ± 0.07	3.15 ± 0.07

TABLE 2

Rate constants and equilibrium constants of some reaction steps in Scheme 1

K_{3a} = M*·ATP/M$^+$·ATP and K_{3b} = M*·ADP·P_i/M*·ATP were calculated from the amplitude of the P_i burst ($K_{app}^{hydrolysis}$ = M*·ADP·P_i/(M$^+$·ATP + M*·ATP)) and the amplitude of the fluorescence enhancement upon ATP binding ($K_{app}^{recovery\ step}$ = (M*·ATP + M*·ADP·P_i)/M$^+$ATP and M*·ATP = $M^*_{(total)}$ − M*·ADP·P_i). All parameters were measured at 20 °C, otherwise stated.

Parameters of Scheme 1	Nucleotide	M_{W501+}	$M_{F481A,\ F482A}$	M_{F652A}
K_1k_{+2} ($\mu M^{-1}s^{-1}$)	ADP	1.50	0.33	0.30
k_{+6} (s^{-1})	mant-ADP	3.5	0.36	0.4
K_1k_{+2} ($\mu M^{-1}s^{-1}$) (6 °C)	ATP	0.80	0.15	0.13
k_{+2} (s^{-1}) (6 °C)		400	170	126
$K_{app}^{recovery\ step}$		5.25	0.27	0.14
$K_{app}^{hydrolysis}$		0.43	0.11	0.05
$K_{3a\ (recovery\ step)}$		2.7	0.14	0.09
$K_{3b\ (hydrolysis)}$		0.55	0.91	0.66
$k_{observed\ hydrolysis}$ (s^{-1})		25.0	5.3	2.2
k_{4+} (s^{-1})		0.05	0.14	0.07

the mutants and the M_{W501+} in the Trp^{501} environment, we performed acrylamide fluorescence quenching experiments. The effect of the acrylamide collisional quenching on the intensity of the fluorescence emission depends on the exposure of the fluorophore to the solvent. We titrated all three constructs with up to 0.4 M acrylamide in the absence and presence of ADP, ATP, and ADP·AlF_4 (supplemental Fig. S2). M_{W501+}·ATP and M_{W501+}·ADP·AlF_4 show significantly decreased Stern-Volmer constants compared with the apo and ADP-bound forms, indicating the more buried tryptophan fluorophore, which is a characteristic of the up lever arm conformation (14). $M_{F481A,\ F482A}$ and M_{F652A} do not show such differences in the Stern-Volmer constants when ATP or ADP·AlF_4 is bound compared with the ADP-bound state (Table 1).

Transient Kinetic Characterization of Trp^{501} Signal Changes—The fluorescence changes of Trp^{501} allowed us to characterize the kinetics of the nucleotide binding steps of $M_{F481A,\ F482A}$ and M_{F652A} in a stopped-flow device and compare them to M_{W501+}. By mixing them with different concentrations of ADP under pseudo-first order conditions, an ~10–15% fluorescence quench was observable in all three constructs. Single exponentials were fitted to the records and the rate constants were plotted as a function of ADP concentration (supplemental Fig. S3). We found that the quenches of the mutants show two-step binding kinetics of an induced fit mechanism as it was described earlier using M_{W501+} (steps 6 and 7 in Scheme 1) (14). The second-order rate constants of ADP binding to the mutants are 5-fold less compared with the wild type (Table 2). Because the ADP off-rates of the mutants also decrease ~10 times as measured by mant-ADP chasing experiments (Table 2 and supplemental Fig. S4), the ADP affinities are only slightly affected by the mutations.

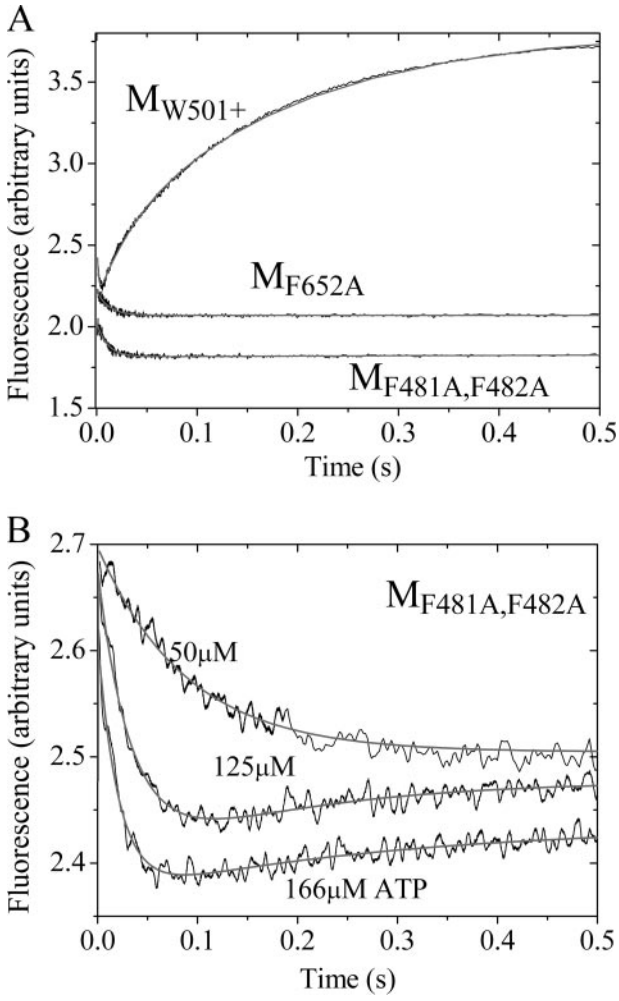

FIGURE 3. **Stopped-flow experiments of ATP binding.** *A*, time course of the fluorescence signal of ATP (1 mM) binding to 3 μM M_{W501+}, $M_{F481A,\ F482A}$, and M_{F652A} at 6 °C. The initial fluorescence quench (K_1K_2 in Scheme 1) can be observed in all cases. *B*, stopped-flow records of ATP binding to $M_{F481A,\ F482A}$ at 20 °C. The fluorescence quench is followed by an increasing phase with a rate constant 5 s^{-1}. In all cases an initial decreasing and a following increase in exponentials were fitted.

ATP binding to M_{W501+} (steps 1 and 2 in Scheme 1) is associated with the same fluorescence quench of Trp^{501} as ADP binding. At 20 °C the subsequent fast recovery step coupled to the fluorescence enhancement does not allow the detection of the transient fluorescence quench. At 6 °C the recovery step slows down compared with the binding event, therefore the fluorescence quench transiently appears in the stopped-flow record (5). Fig. 3*A* shows the ATP binding stopped-flow records of the mutants and that of the M_{W501+} at 6 °C. The fluorescence quenches can be seen in all three cases. The observed rate constants of the fitted exponentials plotted against ATP concentration show that the mutants bind ATP 5 times slower than the M_{W501+} just like in the case of ADP (supplemental Fig. S5*A* and Table 2). The subsequent recovery step coupled to the fluorescence enhancement is detected only in the case of M_{W501+}. At 20 °C, where the high fluorescent state is more populated (based on the emission spectra), both mutants show a small increase ($M_{F481A,\ F482A}$ and M_{F652A}, 3 and 2%, respectively)

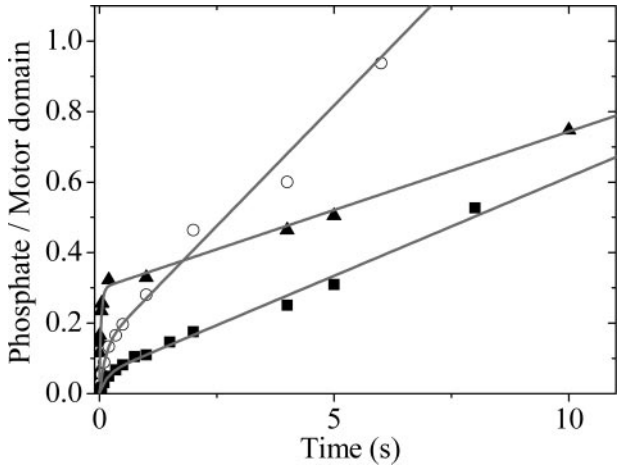

FIGURE 4. **Quench-flow experiments of ATP hydrolysis by M_{W501+} (▲), $M_{F481A,\ F482A}$ (○), and M_{F652A} (■).** 25 μM motor domains were mixed with 180 μM [γ-^{32}P]ATP. The time courses of P_i production show an initial burst phase followed by a steady-state phase in all cases. The relative amplitude of the burst are 0.3, 0.1, and 0.05 in the case of M_{W501+}, $M_{F481A,\ F482A}$, and M_{F652A}, respectively. Kinetic data are presented in Table 2.

after the quench (Fig. 3*B*). At higher ATP concentrations, when the accelerating fluorescent quench has already separated from the enhancement phase, the enhancement phase does not show ATP concentration dependence, the rate constants for $M_{F481A,\ F482A}$ and M_{F652A} are 5 and 2 s^{-1}, respectively. In M_{W501+} the amplitude of the ATP-induced fluorescent enhancement is larger by almost 2 orders of magnitude compared with the mutants. In contrast to the mutants this enhancement has two phases. The first fast enhancement phase is the recovery step (>150 s^{-1}), whereas the second phase is represented by the hydrolysis step ($k_{obs} = (K_{3a}/(1 + K_{3a})) \times k_{3b} + k_{-3b} = 25\ s^{-1}$), which pulls the previous equilibrium toward the high fluorescent M*ATP state (supplemental Fig. S5*B*).

Characterization of the ATP Hydrolysis Steps—The hydrolytic activities of the mutant motor domains were determined by quenched-flow experiments using ^{32}P-labeled ATP (Fig. 4). The experiments were carried out under multiple turnover conditions. All three constructs show a burst phase of the phosphate (P_i) production followed by a steady-state phase, indicating that the observed rate of the ATP hydrolysis step is faster than the rate-limiting step of the enzyme cycle. The amplitude of the burst is three and six times smaller in the case of $M_{F481A,\ F482A}$ and M_{F652A}, respectively, than that of the M_{W501+} (Fig. 4). The steady-state ratio of the pre- and post-hydrolytic states gives the apparent equilibrium constant of the hydrolysis step ($K_{app}^{hydrolysis}$ = M*·ADP·P_i/(M†·ATP + M*·ATP)), which is 4 and 9 times smaller than that of the M_{W501+} (Table 2).

The rate constants of the exponentials fitted to the P_i burst phases of the mutants ($k_{observed\ hydrolysis}$ = 5.3 s^{-1} of $M_{F481A,\ F482A}$, $k_{observed\ hydrolysis}$ = 2.2 s^{-1} of M_{F652A}) are identical to the rate constants of the single phase fluorescence enhancements upon adding ATP. In the case of M_{W501+} the observed rate of the P_i burst phase is identical to that of the second phase of the fluorescence enhancement upon ATP binding (25 s^{-1}).

The rate constants of the steady-state phases of the quenched-flow experiments were slightly faster in the case of the mutants than in that of M_{W501+} (Table 2) and identical to the steady-state turnover rate (k_{4+} in Scheme 1) measured by pyruvate kinase/lactate dehydrogenase-coupled assay.

Determination of K_{3a} and K_{3b}—The fluorescence experiments prove the existence of the down lever arm state of the mutants and a subsequent conformational change that is analogous with the recovery step in the wild type. Furthermore, the quench-flow experiments indicate that the mutants can hydrolyze ATP in this structurally distorted up lever arm state. These findings indicate that the mutations do not change basically the reaction mechanism represented by Scheme 1. According to this scheme three states (M†·ATP, M*·ATP, and M*·ADP·P_i) are populated in the steady-state before the rate-limiting conformational change (step 4) (20). To calculate the steady-state fraction of the low (M†·ADP) and the high ($M^{*}_{(total)}$ = M*·ATP + M*·ADP·P_i) fluorescent states we used the fluorescence intensities of the spectra at the emission maximum (F): ($M^{\dagger} = (F_{ADP\cdot AlF4} - F_{ATP})/(F_{ADP\cdot AlF4} - F_{ADP})$ and ($M^{*} = (F_{ATP} - F_{ADP})/(F_{ADP\cdot AlF4} - F_{ADP})$). The ratio of the high and low fluorescent states gives the apparent equilibrium constant of the recovery step ($K_{app}^{recovery\ step} = M^{*}_{(total)}/M^{\dagger}\cdot ADP$). In the case of $M_{F481A,\ F482A}$ and M_{F652A}, $K_{app}^{recovery\ step}$ is 19 and 38 times smaller than that of M_{W501+} (Table 2). As the steady-state fraction of the M*·ADP·P_i state can be estimated by the relative amplitude of the P_i burst of the quench-flow experiment, the relative population of the three states (M†·ATP, M*·ATP, and M*·ADP·P_i), the equilibrium constants of the recovery step (K_{3a}), and the hydrolysis step (K_{3b}) can be calculated as it shown in Table 2. The greatest perturbation was observed in K_{3a}, which is 20 and 30 times smaller in $M_{F481A,\ F482A}$ and M_{F652A}, respectively, compared with that of M_{W501+}. Although, the P_i bursts of the mutants are also decreased several times, K_{3b} do not show significant differences. It is the consequence of the changed conformation of the up lever arm state that pulls back K_{3a} and hence decreases the P_i burst.

Effects of the Eliminated Pivoting Point in the Presence of Actin—We also investigated the effect of the reduced fulcrum on actin binding. In a stopped-flow device, we determined the observed rate constants of actin binding by mixing pyrene-labeled actin with myosin up to 2 μM in the absence and presence of ADP. The observed rate constants as a function of the myosin concentration were plotted (supplemental Fig. S6) and the on- and off-rates of actin binding were determined ($k_{+A\ and}\ k_{-A}$, respectively, in Table 3) and compared with M_{W501+} (17). They show that the actin affinity ($K_{d,A}$) of $M_{F481A,\ F482A}$ and M_{F652A} compared with M_{W501+} decreased by 10 and 5 times, respectively. As the actin affinity of the mutants weakened similarly in the presence of ADP ($K_{d,DA}$), the thermodynamic coupling ratios did not change significantly.

The ATP-induced actin-myosin dissociation also reveals that the mutations weaken the strengths of the actin-myosin interaction. Myosin preincubated with pyrene-labeled actin was mixed with up to 1 mM ATP in the stopped-flow. The observed rate constants were plotted as a function of the ATP concentration (supplemental Fig. S7). We found that the second-order rate constants of ATP binding and the maximum rate constants of the mutants were several times larger than those of the M_{W501+} (Table 3).

TABLE 3
Kinetic and thermodynamic parameters of the actin-myosin interaction and actin activation

Experiment	Parameter	M_{W501+}	$M_{F481A, F482A}$	M_{F652A}
ATP induced actin-myosin dissociation	K_1k_{+2} ($\mu M^{-1}s^{-1}$) of ATP	0.18	1.3	1.5
	k_{max} (s^{-1})	121	600	700
Actin binding	k_{+A} ($\mu M^{-1}s^{-1}$)	1.60 ± 0.04[a]	0.41 ± 0.05	0.61 ± 0.04
	k_{-A} (s^{-1})	0.047 ± 0.002[a]	0.14 ± 0.01	0.1 ± 0.03
	$K_{d,A}$ (μM)	0.03[a]	0.34	0.16
	k_{+DA} ($M^{-1}s^{-1}$)	0.22 ± 0.02[a]	0.07 ± 0.002	0.12 ±
	k_{-DA} (s^{-1})	0.027 ± 0.002[a]	0.11 ± 0.003	0.108 ± 0.008
	$K_{d,DA}$ (μM)	0.12[a]	1.57	0.90
Actin-activated ATPase activity	v_{max} (s^{-1})	3.8	1.2	1.2
	K_m (μM)	67	61	98

[a] Published in Ref. 17.

We also measured the actin-activated ATPase activities by protein kinase/lactate dehydrogenase-coupled assay (supplemental Fig. S8). We found that the V_{max} values of the mutants are one-third of that of the M_{W501+}, whereas half-saturation (K_m) does not differ significantly (Table 3).

Molecular Dynamics Simulations of the Mutant Motor Domains—Equilibrium molecular dynamics simulations were performed both on the down and up lever arm state structures of the wild type *Dictyostelium* motor domain and on their two mutated forms ($M_{F481A, F482A}$ and M_{F652A}). The *in silico* structural constructs are called similarly to the real mutant constructs with Trp^{501} background, however, they contain all the native tryptophans. The potential energy profiles along the 2-ns long molecular dynamics simulations show that after a few hundred picoseconds all constructs, both in the up and down lever arm states, achieved stable conformations as indicated by an equilibrium phase after the initial potential energy decrease (supplemental Fig. S9). Because the missing relay loop of the $M_{wild\ type}$ down lever arm structure was modeled (Fig. 1*A*), we compared its conformation to that of the scallop myosin structure that contains this region (1KK7) (21), and they have very similar conformations. The down lever arm conformations of the $M_{wild\ type}$ and the mutants do not show significant differences in the structure of the relay helix (Fig. 5*A*). However, in the mutants the up lever arm conformation is unstable and the helical structure at the kink region of the relay helix collapses into a distorted local energy minimum (supplemental Fig. S10), showing that the fulcrum is necessary for the right up lever arm conformation.

We also investigated how the elimination of the pivoting point influences the dynamics of the relay helix in the down lever arm conformations. We collected the main chain torsion angle Φ and Ψ of all residues at each 0.4-ps time point during the equilibrium phases of the molecular dynamics simulations. Fig. 5, *B* and *C*, show the average amplitudes of the torsion angle changes (δ) of the relay helix residues in the down lever arm states. In the relay helix of $M_{wild\ type}$ all torsional angles have very similar mobilities (δ) (similar values to those of other helices in the motor domain) except for Ψ491/Φ492, which is twice as mobile as the others. Plotting these angles in a Ramachandran plot, we can see that Ψ491/Φ492 angles are located even outside of the favored α_R region of a central helix residue (22) unlike the torsion angles of the other residues in the relay helix (supplemental Fig. S11). The mutations have intriguing effects. The mobilities of the Φ and Ψ angles at the perturbed pivoting point are not changed compared with the wild type. However, in $M_{F481A, F482A}$ the amplitudes of the mobilities increased by more than 50% at the positions that are at four (Ψ486/Φ487) and six (Ψ488/Φ489) amino acid positions away from the mutations (481 and 482), whereas Ψ491/Φ492 dropped to half of that of the wild type (Fig. 5*B*). A similar effect was detected in M_{F652A} (Fig. 5*C*). In both mutants Ψ491/Φ492 are located in the α_R region of the Ramachandran plot, whereas Ψ488/Φ489 angles of both mutants tend to move out to a similar region of the Ramachandran plot as the Ψ491/Φ492 are in the wild type (supplemental Fig. S11).

DISCUSSION

In silico simulation of the recovery step suggested that the closure of switch 2 and the rotation of the converter domain are coupled by a seesaw-like movement of the relay helix (9), however, experimental validation of this model is lacking. Fischer *et al.* (9, 11) suggested a two-phase process for the recovery step. In the first phase the N-terminal part of the relay helix moves toward the ATP site and the helix reacts as a seesaw, and consequently it moves the C-terminal to the opposite direction. This movement rotates the lever arm by 25°. In the second phase, the SH1 helix movements provoke a further 40° rotation of the converter and the lever arm. These authors suggested that the latter movement causes an unwinding (or kinking) in the C-terminal region of the relay helix initiated by the break of intra-helical hydrogen bond at 486–490. They explained the order of these two phases by the fact that some necessary side chain rearrangements can only occur in the second phase because they would be hindered sterically as long as the relay helix seesaw motion has not been completed (10). However, such a straightforward structural trajectory between the two structural end states of the recovery step neglects a significant part of the potential conformational space. Recent umbrella sampling simulation on scallop myosin II revealed a large range of possible conformations during the recovery step (23), even states that are far in the conformational space from the main stream of the reaction trajectory suggested by Fischer *et al.* (9). In such a state the SH1 helix unwinding may decouple the converter from the rest of the motor domain (21). The existence of this state seems to be general in myosins (24), however, its role in the recovery step has not been fully understood.

Nevertheless, the seesaw model represents a possible conformational transition leading to the rotation of the lever arm and appoints potential key residues to be investigated experimentally. In this study we made two different mutant constructs ($M_{F481A, F482A}$ and M_{F652A}) with a single Trp^{501} background to

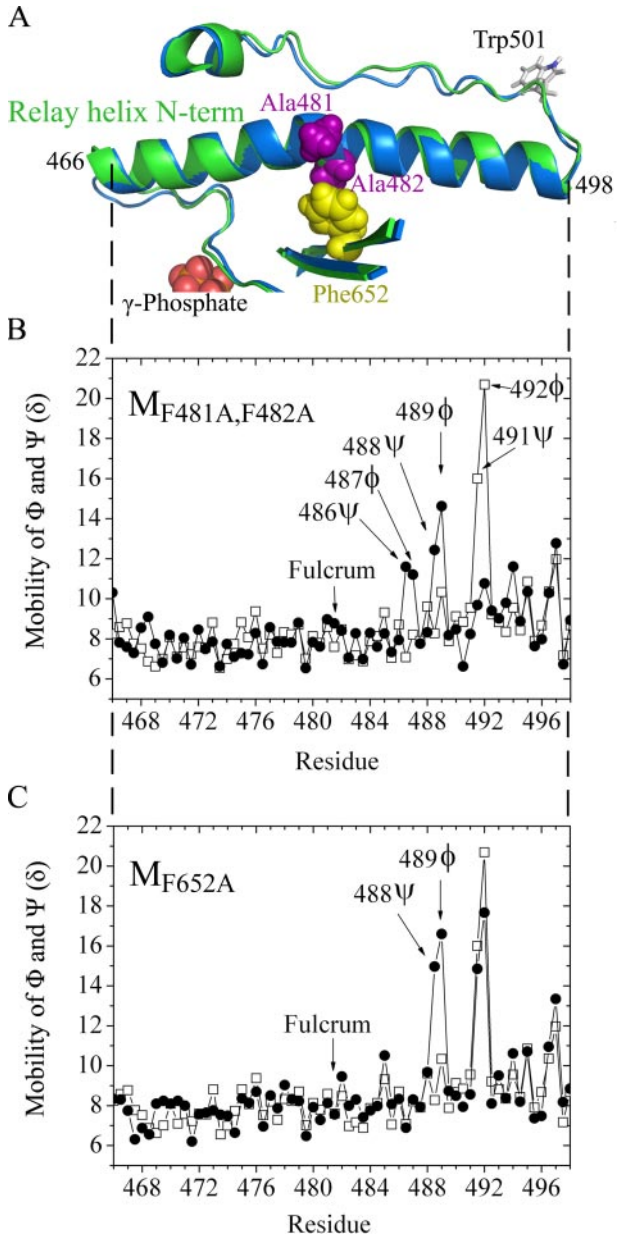

FIGURE 5. **The effect of the deleted fulcrum on the down lever arm structure investigated by molecular dynamics simulation.** *A*, down lever arm conformation of the wild type motor domain before (*green*) and after (*blue*) introduction the mutations F481A and F482A ($M_{F481A, F482A}$). Molecular dynamics simulations were performed on them to achieve local minimum conformations. *B* and *C*, average amplitude of the Φ and Ψ torsion angle changes (δ) in the relay helix during the equilibrium phases of the molecular dynamics simulations of $M_{F481A, F482A}$ (● in *B*) and M_{F652A} (● in *C*) compared with that of the wild type (□ in both). *A* is the structural demonstration of the consecutive residues represented on the *x* axis of *B* and *C*. The two constructs show similar site-specific dynamic changes in the kink region of the relay helix.

perturb the phenylalanine fulcrum of the relay helix (Phe^{481}/Phe^{482}/Phe^{652}) that serves as the pivoting point of the relay seesaw during the recovery step. The results support the essential role of this phenylalanine cluster in the recovery step. The two mutant constructs have astonishingly identical characteristics. They show the same fluorescence states in different nucleotide-bound forms and in the two mutant constructs all reaction steps of the enzyme cycle changed in the same way and magnitude (see Tables 1–3). Both the fluorescence intensities of Trp^{501} and the acrylamide quenching experiments show that the apo and the down lever arm states of the mutants are very similar to the wild type, however, the kinetics of the nucleotide binding are changed to some extent. Additionally, the mutants can hydrolyze ATP despite the changed up lever arm state conformation. It indicates that switch 2 is closed in that conformation like in the wild type, because correct closed conformation of switch 2 is required for the effective hydrolysis as it was previously demonstrated (15, 16). However, the smaller Trp^{501} fluorescence increases of the mutants upon ADP·AlF_4 binding indicate that the conformation of the distal part of the relay helix is perturbed in that changed up recovery state. Hence, the lack of the phenylalanine fulcrum diverts the relay helix into a changed conformation upon switch 2 closure. It is also indicated by the dramatically suppressed equilibrium constants of the recovery step. Acrylamide quenching experiments show that this changed conformational state resembles the down lever arm state of the relay helix as Trp^{501} remains on the surface of the motor domain, as in the down lever arm orientation (14). Hence, it is also likely that, although switch 2 closes, the converter/lever arm region remains in a down lever arm-like orientation and the relay seesaw cannot tilt in the absence of its pivoting point. In other words the lack of the fulcrum decouples the distal part of the relay helix from the nucleotide binding site upon the recovery step.

Our molecular dynamic simulations are consistent with the conclusions derived from the experimental data. Although the up lever arm states of both mutants are distorted in the kink region of the relay helix, the down lever arm states do not show significant structural differences compared with the wild type (supplemental Fig. S10 and Fig. 5). However, the mutations changed the dynamics of the pre-recovery relay helix. In the wild type the mobility of the backbone is relatively low along the relay helix, except for a highly mobile part (Ψ491/Φ492) in the kink region (Fig. 5*B*). These residues are not just highly mobile, but the Ψ491/Φ492 torsion angles are located outside of the favored α_R region of a central helix residue. These properties indicate that this part of the kink region is strained in the down lever arm state. In the mutants this strained part of the kink region is shifted by a few amino acids (Ψ486/Φ487 and Ψ488/Φ489), indicating that the elimination of the fulcrum rearranges strains along the relay helix. It is an interesting question how the strain distribution changes along the reaction trajectory of the recovery step leading to unwinding of the relay helix in the second phase. In the first phase the tilt of the helix might increase the tension in the kink region in which the phenylalanine fulcrum has an active role.

As we recently demonstrated, the rate-limiting step of the basal ATPase cycle of *Dictyostelium* myosin II is the reverse recovery step in ADP·P_i (k_4) (20). Therefore actin has to activate this reversal lever arm swing. However, the molecular mechanism that drives the activation of the lever arm movement when actin cleft closes is not known yet. If the power stroke is induced through the relay helix, a plausible explanation could be that cleft closure somehow lifts back the relay seesaw (by pushing the N-terminal end of the relay helix to its pre-recovery conformation), leading to the destabilization of the kinked conforma-

tion of the helix and to the rotation of the converter/lever arm region. Based on the rigor-like structure of myosin V, Coureux *et al.* (25) suggested that cleft closure induces the bending of the central β-sheet (especially the strands that carry switches 1 and 2), which opens the nucleotide pocket. Switch 2 opening might be able to lift back the relay helix to its pre-recovery orientation, however, a direct communication mechanism between the actin binding regions and the lever arm has not been revealed, yet.

The mutational analysis proved that the seesaw model of the recovery step can be a basic mechanism that transforms the movement of the switch 2 loop to the rotation of the converter/lever arm region and the pivoting point of the seesaw is essential to this movement, as it was suggested by Fischer *et al.* (9). The lack of it hinders this movement and decouples the lever arm rotation from the other functions of the motor domain. However, the mutation of the pivoting point also affects actin and nucleotide binding. These findings suggest a complex work of the relay as it determines the movement of the lever arm and also influence the processes of other functional regions of the motor domain.

Acknowledgments—We thank Stefan Fischer for critical reading, Jon Kull for the coordinates of the up lever arm state structure containing all residues, Prof. Mike A. Geeves, David S. Person, Andrea Fejér, Judit Tóth, and Jiannan Feng for help.

REFERENCES

1. Conibear, P. B., Bagshaw, C. R., Fajer, P. G., Kovacs, M., and Malnasi-Csizmadia, A. (2003) *Nat. Struct. Biol.* **10,** 831–835
2. Holmes, K. C., Angert, I., Kull, F. J., Jahn, W., and Schroder, R. R. (2003) *Nature* **425,** 423–427
3. Kintses, B., Gyimesi, M., Pearson, D. S., Geeves, M. A., Zeng, W., Bagshaw, C. R., and Malnasi-Csizmadia, A. (2007) *EMBO J.* **26,** 265–274
4. Reubold, T. F., Eschenburg, S., Becker, A., Kull, F. J., and Manstein, D. J. (2003) *Nat. Struct. Biol.* **10,** 826–830
5. Malnasi-Csizmadia, A., Pearson, D. S., Kovacs, M., Woolley, R. J., Geeves, M. A., and Bagshaw, C. R. (2001) *Biochemistry* **40,** 12727–12737
6. Urbanke, C., and Wray, J. (2001) *Biochem. J.* **358,** 165–173
7. Fisher, A. J., Smith, C. A., Thoden, J. B., Smith, R., Sutoh, K., Holden, H. M., and Rayment, I. (1995) *Biochemistry* **34,** 8960–8972
8. Geeves, M. A., and Holmes, K. C. (2005) *Adv. Protein Chem.* **71,** 161–193
9. Fischer, S., Windshugel, B., Horak, D., Holmes, K. C., and Smith, J. C. (2005) *Proc. Natl. Acad. Sci. U. S. A.* **102,** 6873–6878
10. Koppole, S., Smith, J. C., and Fischer, S. (2007) *Structure* **15,** 825–837
11. Mesentean, S., Koppole, S., Smith, J. C., and Fischer, S. (2007) *J. Mol. Biol.* **367,** 591–602
12. Yu, H., Ma, L., Yang, Y., and Cui, Q. (2007) *PLoS Comput. Biol.* **3,** e23
13. Yu, H., Ma, L., Yang, Y., and Cui, Q. (2007) *PLoS Comput. Biol.* **3,** e21
14. Malnasi-Csizmadia, A., Woolley, R. J., and Bagshaw, C. R. (2000) *Biochemistry* **39,** 16135–16146
15. Bauer, C. B., Holden, H. M., Thoden, J. B., Smith, R., and Rayment, I. (2000) *J. Biol. Chem.* **275,** 38494–38499
16. Holmes, K. C., and Geeves, M. A. (2000) *Philos. Trans. R. Soc. Lond. B Biol. Sci.* **355,** 419–431
17. Gyimesi, M., Tsaturyan, A. K., Kellermayer, M. S., and Malnasi-Csizmadia, A. (2008) *Biochemistry* **47,** 283–291
18. Toth, J., Varga, B., Kovacs, M., Malnasi-Csizmadia, A., and Vertessy, B. G. (2007) *J. Biol. Chem.* **282,** 33572–33582
19. Trentham, D. R., Bardsley, R. G., Eccleston, J. F., and Weeds, A. G. (1972) *Biochem. J.* **126,** 635–644
20. Gyimesi, M., Kintses, B., Bodor, A., Perczel, A., Fischer, S., Bagshaw, C. R., and Malnasi-Csizmadia, A. (2008) *J. Biol. Chem.* **283,** 8153–8163
21. Himmel, D. M., Gourinath, S., Reshetnikova, L., Shen, Y., Szent-Gyorgyi, A. G., and Cohen, C. (2002) *Proc. Natl. Acad. Sci. U. S. A.* **99,** 12645–12650
22. Ho, B. K., Thomas, A., and Brasseur, R. (2003) *Protein Sci.* **12,** 2508–2522
23. Harris, M. J., and Woo, H. J. (2008) *Eur. Biophys. J.*, in press
24. Liang, W., and Spudich, J. A. (1998) *Proc. Natl. Acad. Sci. U. S. A.* **95,** 12844–12847
25. Coureux, P. D., Wells, A. L., Menetrey, J., Yengo, C. M., Morris, C. A., Sweeney, H. L., and Houdusse, A. (2003) *Nature* **425,** 419–423
26. Berendsen, H. J. C., Postma, J. P. M., Gunsteren, W. F., DiNola, A., and Haak, J. R. (1984) *J. Chem. Phys.* **81,** 3684